INTERNATIONAL JOURNAL OF PRECISION ENGINEERING AND MANUFACTURING Vol. 17, No. 7, pp. 845-855 JULY 2016 / 845
DOI: 10.1007/s12541-016-0103-z ISSN 2234-7593 (Print) / ISSN 2005-4602 (Online)

Tool-Wear Monitoring during Micro-End Milling using Wavelet Packet Transform and Fisher's Linear Discriminant

Young-Sun Hong[1], Hae-Sung Yoon[2,3], Jong-Seol Moon[1], Young-Man Cho[2,#], and Sung-Hoon Ahn[1,2,#]

1 Department of Mechanical and Aerospace Engineering, Seoul National University, 1 Gwanak-ro, Gwanak-gu, Seoul, 08826, South Korea
2 Institute of Advanced Machines and Design, Seoul National University, 1 Gwanak-ro, Gwanak-gu, Seoul, 08826, South Korea
3 BK21 Plus Transformative Training Program for Creative Mechanical and Aerospace Engineers, Seoul National University, 1 Gwanak-ro, Gwanak-gu, Seoul, 08826, South Korea
Corresponding Author / E-mail: ahnsh@snu.ac.kr, TEL: +82-2-880-7110, FAX: +82-2-888-9073
E-mail: ymcho85@hotmail.com, TEL: +82-2-886-9074, FAX: +82-2-888-9073

KEYWORDS: Condition monitoring, Hidden Markov model, Micro end mill, Single-period signal, Tool lifespan, Wavelet packet transform

Tool wear is one of the most important parameters in micro-end milling, and can be used to monitor the condition of the machine and the tool. A micro-end mill has different characteristics from a macro-scale end mill; in particular, shank run-out (which is negligible in the macro-scale tool due to the low aspect ratio) is significant in micro-end milling, inducing excessive tool wear and reduced tool life and leading to sudden, premature failure. In this paper, a novel tool-wear monitoring method is described for determining the state of a micro-end mill using wavelet packet transforms and Fisher's linear discriminant. Force and torque signals were measured using a dynamometer and were used to reflect geometric changes in the micro-end mill due to wear. Because of the small signal-to-noise ratio, sensor signals measured during the milling process were periodically averaged, and the resulting single-period signals provided improved efficiency of feature extraction using wavelet packet transforms. The extracted features were classified in the wavelet domain and used to determine the tool state employing a hidden Markov model. The recognition results were compared with those of an energy-based monitoring technique, and we found that our method could determine the tool state more accurately for both normal wear and premature failure of micro-end mills.

Manuscript received: November 5, 2014 / Revised: January 3, 2016 / Accepted: March 16, 2016

1. Introduction

Tool wear is one of the most important parameters for monitoring the tool state in micro-end milling, and is directly related to the machining quality.[1] Direct, continuous observation of the tool and workpiece quality is not readily accomplished during machining; hence indirect techniques employing various sensor signals are typically used to determine the tool state.[2-5] It is more difficult to monitor the tool state with a micro-end mill than with a macro-scale tool, because the measured signal is small and hence is buried by noise.[6,7] Additionally, sudden failure at the flute may occur due to the small tool diameter.[8-10]

To overcome these problems, tool-wear monitoring is required for micro-end mills. Moreover, due to the high speed of the machining processes and the use of micro-scale tools, high-resolution sensors and advanced signal processing methods are required to extract the features related to tool wear. Monitoring focuses on changes in the tool wear over time because the tool state is typically defined in terms of geometrical changes in the tool.

Various sensor signals are used in tool wear monitoring, including force, torque, and acoustic signals emitted during end milling, and signal processing techniques are applied to extract salient data from the raw signals.[11-13] Analyses of the time and frequency domains are used for feature extraction, and the selected features can applied to determine the tool state using pattern recognition methods, such a hidden Markov model (HMM), artificial neural network, or support vector machine.[14] Feature extraction typically focuses on the energy of the measured signal, the filtered signal, or the transformed coefficient.

In micro-end milling, where the tool wear is often $<20\ \mu m$, the relevant features can be difficult to extract from the signal because of the small signal-to-noise ratio (SNR), or they may only be contained in some specific range of the signal. Single-period signals, in which a measured signal is split into periodic components with the same period

as the rotation period of the spindle, allow a wear symptom in a measured signal to be detected more easily because the signal should appear periodically. Tool wear monitoring that focuses on wear symptom detection in a single-period signal improves the efficiency of feature extraction and tool state clustering compared with energy-based monitoring methods.

Because of the high aspect ratio of the tool bit, run-out has a more significant effect on rotational behavior in micro-end milling than in macro-scale end milling, leading to tool wear imbalance and thereby shortening the lifespan of the tool. Single-period tool analysis can reveal the relationship between wear imbalance and tool life and enables tool wear monitoring to anticipate sudden failures. In the micro machining, the measured signals were very weak, and it could be buried by the environmental noise. Wavelet packet transform (WPT) has advantage in detection of fault symptom from the measured weak signal using various basis and the subdivided frequency range. Also, in order to reduce the diagnosis error, probabilistic estimation technique was adopted. Using the HMM, diagnostic results were consider using the not only the observed sensor signal but also previous state history.

In this paper, we describe a novel tool wear monitoring method based on single-period signal analysis that uses a WPT and an HMM to characterize tool run-out. The mechanical behavior of a micro-end mill with tool run-out is investigated in terms of the tool life, the imbalance torque, and the time variation in the torque. WPT and Fisher's linear discriminant were used to extract features from measured machining signals, and HMM was applied to tool state recognition depending on the tool wear (*i.e.*, machining distance).

2. Condition Monitoring

2.1 Shank run-out

Because the diameter of a micro-tool is small, shank run-out is a particularly significant problem.[15,16] Shank run-out not only induces unbalanced rotary motion and tool wear imbalance but also shortens the tool life.

Shank run-out of a cutting tool leads to machined features that are larger than the tool diameter due to unbalanced tool rotation. This is caused by imperfect tool alignment, asymmetric tool geometry, mismatch between the tool and the tool holder, and vibrations during machining.[17] Because of the small magnitude of shank run-out, it can often be neglected in macro-scale machining; however, because of the high aspect ratio and small tool diameter in micro-end milling, run-out is more significant and affects the machining signals, wear, and tool life.[18] Shank run-out can be measured using a dial gauge, with the total indicator reading (TIR) value defined as follows:

$$TIR = \frac{|\max(\text{gauge value}) - \min(\text{gauge value})|}{2} \quad (1)$$

2.2 Strategy for tool wear monitoring

The force and torque signals can accurately reflect the machining state, and the measured force signals correspond to differences in micro-end milling behavior due to varying shank run-out effects, as shown in Fig. 1.

The force signals during micro-end milling were recorded at machining distances of 0 m and 0.8 m. Fig. 1(a) shows the force signals with small run-out; the waveforms are similar between the two machining distances.

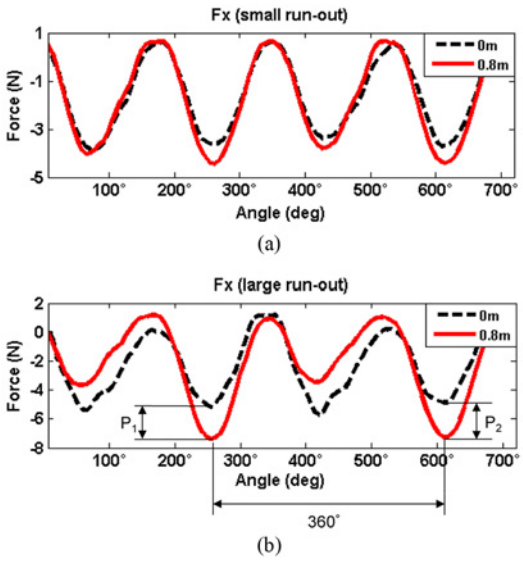

Fig. 1 The *x*-axis force signals during end milling (a) with a small run-out and (b) with a large run-out. P1 and P2 denote the differences in the maximum force between machining distances of 0 m and 0.8 m.

Fig. 1(b) shows the force with larger run-out; the imbalance at 0.8 m was larger than that at 0 m because of the large run-out, and the maximum difference in force between the two machining distances was repeated at 360° intervals (*i.e.*, periodically with the rotation of the tool). The geometric changes in the tool due to increased machining distance (and hence tool wear) affect the machining signal.

In micro-machining, variations in machining signals with respect to machining distance are weak compared with those in macro-scale machining. The energy parameters, including the mean, peak, standard deviation, kurtosis, and skewness, of the measured signal, cannot reflect these slight variations due to increased machining distance, as shown in Fig. 1(b). Therefore the machining distance (*i.e.*, tool wear) at which the maximum difference appears more accurately reflects the state of a micro-end milling tool.

3. Theoretical Background

3.1 Wavelet packet transform

A wavelet transform is a convolution between a signal $f(t)$ and a daughter wavelet $\psi_{a,b}(t)$, which is modified from a mother signal $\psi(t)$ via a dilatation a and translation b, and where $\psi(t)$ is modified from the mother signal $f(t)$.[19] The continuous form of the wavelet transform is as follows:

$$W_\psi f(a,b) = \langle f(t), \psi_{a,b}(t) \rangle = \frac{1}{\sqrt{a}} \int_{-\infty}^{\infty} f(t) \psi\left(\frac{t-b}{a}\right) dt \quad (2)$$

A continuous wavelet transform (CWT) incurs substantial computational expense and also leads to the creation of redundant terms. To overcome this, the discrete wavelet transform (DWT) can be

used to analyze the signal, which is based on a dyadic form of dilatation and translation (*i.e.*, $a=2^j$, $b=k2^j$), and is defined as follow:

$$W_\psi f(2^j,k2^j) = \langle f(t), \psi_{2^j,k2^j}(t)\rangle = \frac{1}{\sqrt{2^j}}\int_{-\infty}^{\infty} f(t)\psi\left(\frac{t-k2^j}{2^j}\right)dt \quad (3)$$

where j is the scale and k is the translation variation. With DWT, the wavelet and scaling functions are applied to the signal as low-pass and high-pass filters, respectively. The wavelet and scaling functions are defined as follows:

$$\phi_{j+1,p} = \sum_{n=-\infty}^{+\infty} h[n-2p]\phi_{j,p} \quad (4)$$

$$\psi_{j+1,p} = \sum_{n=-\infty}^{+\infty} g[n-2p]\phi_{j,p} \quad (5)$$

where $g[n]=(-1)^{1-n}h[1-n]$, $h[n-2p]$ and $g[n-2p]$ are filter coefficients of the low-pass and high-pass filter, respectively, and p is the filter length. Using the above expressions, each wavelet coefficient $a_j[n]$ can be decomposed into compact frequency ranges, namely a low-frequency term $a_{j+1}[p]$ and a high-frequency term $d_{j+1}[p]$, *i.e.*,

$$a_{j+1}[p] = \sum_{n=-\infty}^{+\infty} h[n-2p]a_j[n] \quad (6)$$

$$d_{j+1}[p] = \sum_{n=-\infty}^{+\infty} g[n-2p]a_j[n] \quad (7)$$

DWT only analyzes the low-frequency terms, and hence the features in the high-frequency terms are neglected. To cover the entire frequency range, the WPT, which is an expanded version of the DWT, was used to analyze the signal throughout the low- and high-frequency ranges simultaneously. The wavelet packet bases at the child nodes are defined as follows:

$$\psi_{j+1}^{2p} = \sum_{n=-\infty}^{+\infty} h[n]\psi_j^p(t-2^j n) \quad (8)$$

$$\psi_{j+1}^{2p+1} = \sum_{n=-\infty}^{+\infty} g[n]\psi_j^p(t-2^j n) \quad (9)$$

Where p is the number of nodes, and j is the level in the wavelet tree. The wavelet packet coefficients were computed via the convolution integral between the signal and the two-channel filter bank, *i.e.*,

$$d_j^p[n] = \langle f(t), \psi_j^p(x-2^j n)\rangle \quad (10)$$

Because the computed wavelet packet coefficients reflect the signal and the daughter wavelet (*i.e.*, the base), they can be changed by varying the base. Several cost functions were used to choose the optimal base to extract the features of interest. The chosen base can be used to identify many features that are relevant for monitoring tool wear.[20]

3.2 Hidden Markov model

A hidden Markov model is a doubly stochastic process, with an underlying stochastic process that is not directly observable and can only be observed via another set of stochastic processes that produce a sequence of observed symbols.[21,22] The N hidden states $S=\{S_1, S_2, \ldots, S_N\}$ are tool states, and the M observation sequences $O=\{O_1, O_2, \ldots, O_M\}$ are machining signals during micro-end milling.[23,24] An HMM is described by the model $\lambda = (A, B, \pi)$, in which

- $A = \{a_{ij}\}$ is the state transition probability distribution, where $a_{ij} = P[q_{t+1}=S_j \mid q_t=S_i]$, and the state at time t is q_t. $A = \{a_{ij}\}$ is a probability of state S_j following state S_i.
- $B = \{b_j(k)\}$ is an observation symbol probability distribution in state j, where $b_j(k) = P[O_k \text{ at } t \mid q_t = S_j]$.
- $\pi = \{\pi_i\}$ is an initial state distribution where $\pi_i = P[q_1=S_i]$.

If the observations are continuous signals, the discrete probabilities are replaced with continuous probability distribution function, which is generally approximated by a weighted sum of M Gaussian distribution η, *i.e.*,

$$b_j(O_t) = \sum_{m=1}^{M} c_{jm}\eta(\mu_{jm}, U_{jm}, O_t) \quad (11)$$

where c_{jm} is a weighting coefficient, μ_{jm} is the mean vector, U_{jm} is a covariance matrix, and M is the number of components.[25] The model with a continuous distribution is given by

$$\lambda = (A, c_{jm}, \mu_{jm}, U_{jm}, \pi) \quad (12)$$

4. Feature Extraction using Wavelet Packet Transform and Fisher's Discriminant

Data on tool wear can be extracted from the machining signals, and a wavelet packet transform was applied to detect the features of interest. The wavelet coefficients were extracted from the signals according to the machining distance using WPT. The wavelet coefficients were determined by selecting the daughter wavelet, *i.e.*, the base. For this reason, the selection of a base is important to classify the state of the micro-end mill according to the tool wear or machining distance.

Each base was evaluated using Fisher's linear ratio, which can be used to differentiate between groups and allows us to focus on a particular group. The Fisher's discriminant ratio (FDR) is defined as follows

$$FDR = \frac{|m_{normal} - m_{wear}|^2}{\sigma_{normal} + \sigma_{wear}} \quad (13)$$

where m is the mean and σ is the standard deviation of coefficients. The means and standard deviations of the normal- and wear-state groups of the tool were used for classification and concentration of the wavelet coefficients. A large FDR means that the two groups are well differentiated, and each coefficient is concentrated within the group. Fig. 2 shows the application for the force data due to tool wear.

The machining signals reflect the tool state, and groups of signals with different machining distances (*i.e.*, different tool wear) were analyzed using WPT and FDR to obtain a base for discriminating between different groups. The optimal base was then used to generate the wavelet coefficients used to diagnose the signal state. All bases contain information on the daughter wavelet, level, node, and translation; higher-level analysis provides greater accuracy but also requires more computational time. The periodic signals were preprocessed to divide the original signal into multiple single-cycle signals.

Fig. 3 illustrates the choice of the optimal base using FDR when

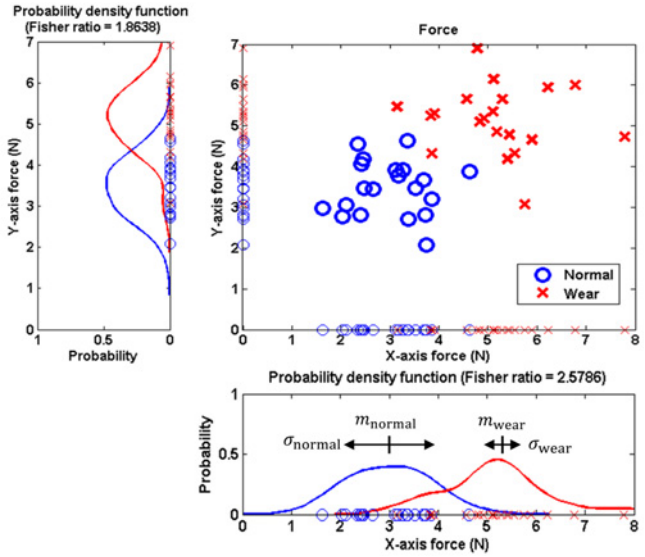

Fig. 2 Fisher's linear discriminant for the force data with different tool wear

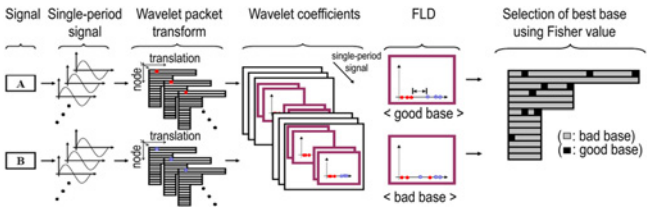

Fig. 3 Condition-monitoring method for a micro-tool using WPT and Fisher's linear discriminant (Adapted from Ref. 26 with permission)

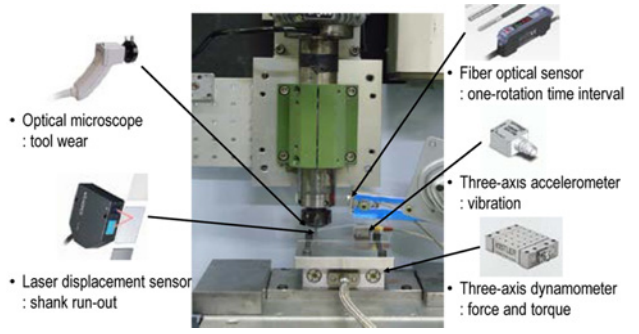

Fig. 4 A photograph showing the micro-end milling experimental setup

two states are to be classified. In this analysis, single-period signals of each state are used for detection, so the measured signals from the micro-end mill were divided using a single-period time interval and acquired via an optical fiber sensor.

Each single-period signal was resampled to have the same data length for the WPT analysis because the single-period time intervals may differ slightly. The resampling compensates for the data length variations. Fig. 3 shows signals for the two states, *i.e.*, normal (A) and wear (B). The signals of the two states were resampled to generate multiple single-period signals, and the wavelet coefficients were estimated using FDR for simultaneous classification and concentration.

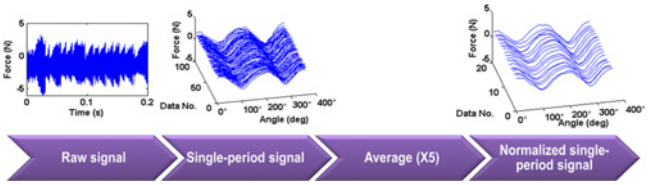

Fig. 5 Signal post processing

Some bases can be used to separate the groups completely, whereas other cannot separate the groups effectively. The separation depends on the ability of the base that is selected to differentiate between the two groups. A good base generates wavelet coefficients that are well clustered and are separated according to the state, whereas a poor base does not. The gray region in the rightmost part of Fig. 3 corresponds to poor bases, and the black region represents good bases that produce two isolated groups of wavelet coefficients, which correspond to the two different states. Once good candidate bases have been identified, the optimal base is chosen from among them by evaluating the FDR. (The optimal base is the one that maximizes FDR.) Using this base, the measured signals for each state can be classified and concentrated simultaneously.[26]

5. Experimental Setup

The experimental setup is shown in Fig. 4. The workpiece was a 80 × 120 × 1-mm sheet of Al-5052 aluminum alloy. The micro-end mill had two flutes, and the diameter was 500 μm. The machining signals for tool wear monitoring were sampled via a data acquisition board (CP-1103, dSPACE GmbH, Germany) at a sampling frequency of 20 kHz with a 9-kHz low-pass filter for antialiasing. The tool wear was measured using a digital microscope (ICS-305B, Sometech Vision Co., Ltd., Korea) at 0.08-m intervals in the machining distance.

Shank run-out was measured using a laser displacement sensor (LK-G3000, Keyence, Japan) with no load and a spindle speed of 100 Hz, and the period of tool rotation was measured using an optical-fiber sensor (FU-35FA, Keyence, Japan). The cutting force and torque were measured with a 5-channel dynamometer (Type 9256C1, Kistler Instrumente AG, Switzerland), and the workpiece was mounted as shown in Fig. 4. Workpiece vibrations were measured using a tri-axial accelerometer (3093B13, Dytran Instruments, Inc., USA).

5.1 Signal post-processing

The raw data were split into single-period time intervals using the fiber-optic sensor to generate the single-period signals. Each single-period signal was averaged five times. The signal post-processing dataflow is shown in Fig. 5.

5.2 Clamping torque

Shank run-out can be caused by imperfect tool alignment, asymmetric tool geometry, mismatch between the tool and tool holder, and tool vibration during machining. In micro-end milling, shank run-out creates

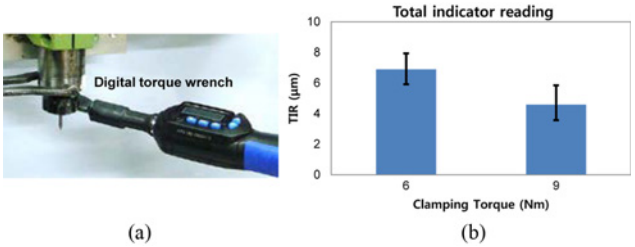

Fig. 6 (a) Clamping of the micro-end mill to the spindle chuck using a digital torque wrench, (b) TIR data for different clamping torques

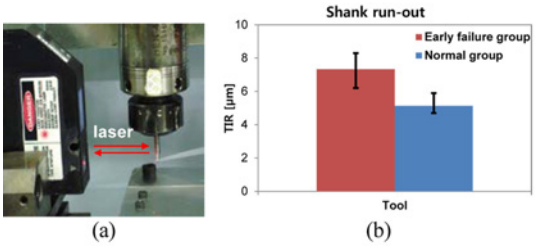

Fig. 7 (a) Measurement of shank run-out using the laser displacement sensor and (b) the tool life according to shank run-out. The spindle speed was 100 Hz.

a rotational imbalance and affects the lifespan and wear mode of the tool. Unbalanced rotation increases the cutting force and tool wear (which is directly related to tool lifespan). To minimize shank run-out caused by tool attachment, a constant clamping torque was applied between the micro-end mill and the chuck using a digital torque wrench.

Shank run-out was observed using the laser displacement sensor for clamping torques of 6 and 9 Nm, as shown in Fig. 6. The TIR for a clamping force of 9 Nm was smaller than that for a force of 6 Nm. It follows that the clamping force affects shank run-out. The larger clamping torque reduced the variation in shank run-out. Therefore, the clamping torque was set at 9 Nm in the following experiments.

5.3 Tool life with shank run-out

Shank run-out affects the tool life and mechanical behavior of a micro-end mill. The laser displacement sensor measurements of shank run-out without load and before end milling are shown in Fig. 7(a). The resolution of the laser displacement sensor was in the range 0.2 μm ~ 1 mm; however, the environmental noise interfered with the measurement. To minimize the effects of noise, a low-pass filter was applied to the signal, and we extracted only the frequency components below 200 Hz. The filtered TIR and lifespan of each micro-end mill were compared. In this experiment, two tool-life groups were observed depending on the TIR. The early failure group had failed with a total machining distance of <0.5 m, whereas the typical machining distance for the normal group was ~0.96 m. As shown in Fig. 7(b), the group with TIR <6 μm (*i.e.*, the normal group) had long tool lives compared with the group with TIR >6 μm (early failure group).

5.4 Torque imbalance ratio and the maximum torque due to shank run-out

The single-period signals from the premature failure group and the normal group were analyzed, as shown in Fig. 8. The tool from the early failure group failed after 0.48 m, whereas the tool from the normal group did not fail after a machining distance of 0.96 m on average.

There are two peaks in the single-period signal shown in Fig. 8(a), and the peak values increased with increasing machining distance (*i.e.*, tool wear). However, the difference between the two peaks did not change. In the normal group, the torque was smaller than in the premature early group, and the torque waveform was very uniform, as indicated by the small peak differences. It follows that shank run-out affects not only the torque waveform but also the cutting torque. The two peaks A1 and A2 or (A'1 and A'2) indicate that the difference in the cutting torque due to contact between the micro-end mill edges and the workpiece generates imbalance that produces eccentric rotary motion of the tool. Because of this eccentric rotary motion, one edge of the micro-end mill cuts a larger volume of the workpiece than the other does. The torque imbalance ratio directly relates to the tool run-out and is defined as follows:

$$\text{Imbalance torque ratio} = \frac{A_1}{A_2} \text{ or } \frac{A'_1}{A'_2} \tag{14}$$

Stress concentration appears at one edge, and the eccentric behavior increases the torque imbalance. Thus, the tool life decreases over the entire machining distance due to the excessive torque imbalance ratio concentrates torque on one edge of the micro-end mill, as shown in Fig. 8(c), which leads to faster tool wear.

In the early failure group, the tool life was shorter than that in the normal group because of the stress concentration at one edge. The torque imbalance ratio did not change rapidly with the machining distance. Torque imbalance also leads to increased maximum torque, as shown Fig. 8(d). The two groups of tools showed a difference in the evolution of the torque with machining distance. In the early failure group, the maximum torque increased rapidly, whereas in the normal group, the maximum torque varied more slowly.

5.5 Tool wear due to shank run-out

Tool wear was observed using an optical microscope at 0.08-m intervals in machining distance. The tool wear for both the early failure group and the normal group is shown in Fig. 9(a). For the early failure group, the tool wear at a machining distance of 0.48 m was larger than that for the normal group at a machining distance of 0.96 m. It follows that shank run-out affects not only tool wear but also the life of the micro-end mill.

The overall wear is summarized in Fig. 9(b). The tool wear of the early failure group increased rapidly with the machining distance and exceeded 30 μm before the machining distance reached 0.5 m. The normal group exhibited a more gradual increase in tool wear as a function of the machining distance, and the maximum wear was <30 μm at a machining distance of 0.96 m.

The torque imbalance ratio was determined as a function of the shank run-out. The torque imbalance ratio causes the torque to be concentrated more at one edge than at the other. Eventually, this torque concentration increases the maximum torque, thereby decreasing the tool life.

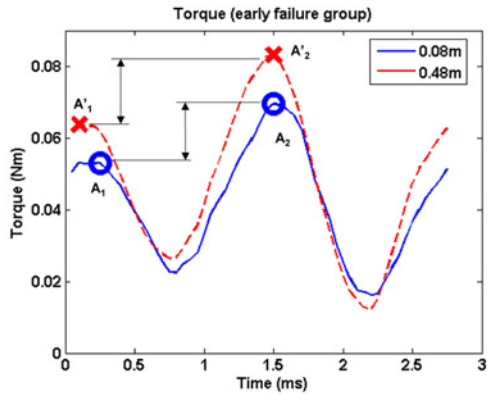

(a)

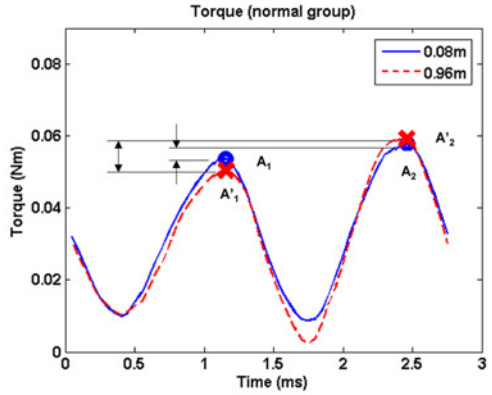

(b)

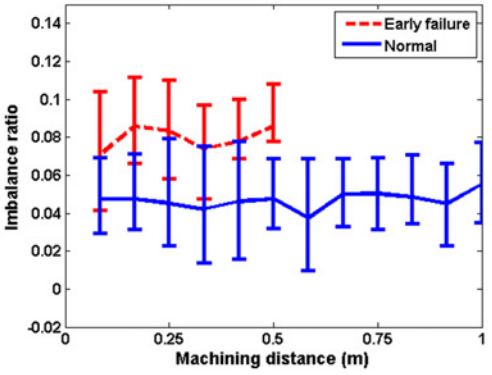

(c)

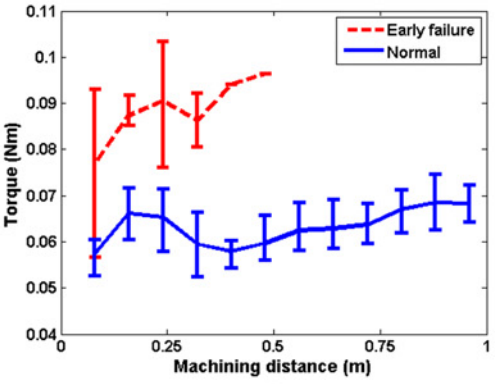

(d)

Fig. 8 (a) Torque imbalance of the early failure group, (b) Torque imbalance of the normal group, (c) The torque imbalance ratio as a function of machining distance, (d) Maximum torque of the early failure and normal groups as a function of the machining distance

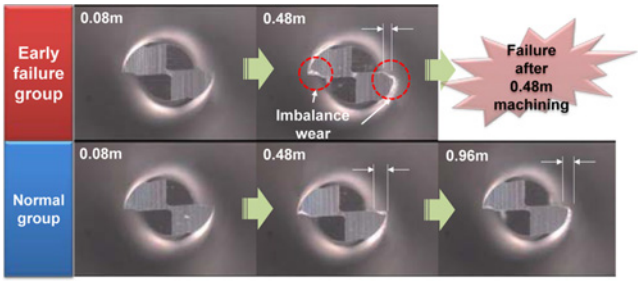

(a)

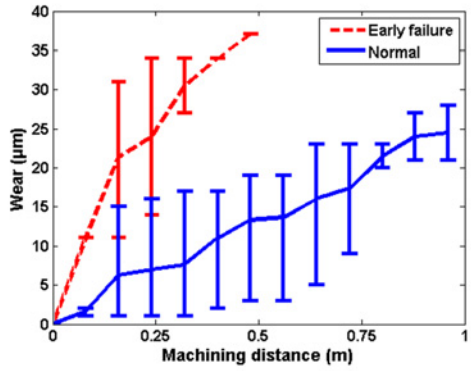

(b)

Fig. 9 Micro-end mill wear: (a) Optical microscope images of the early-failure group and the normal group (b) Overall wear aspects of the two groups with machining distance

6. Condition Monitoring

6.1 Classification using the component-level method

The optimal bases for the torque and force signals were used to monitor tool wear, as listed in Tables 1 and 2. Data at machining distances of 0.08 m and 0.48 m were used to select the optimal base, and data at 0.96 m were applied to the chosen base for state classification in the wavelet domain. Because the abnormal peak position was not fixed throughout the machining process in a single-period signal, data for the initial and middle stages of machining were used to determine the optimal base for revealing features related to tool wear at different machining distances. It follows that the abnormal peak in the single-period signal increased with increasing tool wear.

The classification results for the force data at 0.08 m and 0.48 m are shown in Fig. 10(a). The two groups were well classified in the wavelet domain, and using the same optimal base, the untrained data (*i.e.*, force data at 0.96 m) were applied to the wavelet domain. As shown in Fig. 10(b), the untrained data were also well classified, and tended toward larger values in the wavelet domain. This means that the wavelet features generated using the optimal base increased with machining distance.

Using these wavelet features, the state of a micro-end mill can be classified in the wavelet domain. Moreover, the untrained data (*i.e.*, after a machining distance of 0.96 m) can be applied to the same optimal base (which was chosen at machining distances of 0.08 m and 0.48 m), and the resulting data were clustered in the wavelet domain. Figs. 10(c) and 10(d) show the classification results using the torque data; each state was well classified in the wavelet domain.

Table 1 Optimal base for the force data

Best base	1st	2nd
Wavelet	db6	db7
Level	3	3
Node	2	2
Translation	1	5

Table 2 Optimal base for the torque data

Best base	1st	2nd
Wavelet	db3	db6
Level	3	3
Node	1	2
Translation	4	3

Data for various machining distances were applied to optimal bases that were generated at machining distances of 0.08 m and 0.48 m. The resulting classifications are shown in Figs. 11(a) and 11(b). Some coefficients interfered with each other; however, the group was well classified in the wavelet domain using the chosen bases. It follows that these bases can be used to classify the state of the tool in the wavelet domain over the entire range of machining distances.

6.2 Component-level analysis

The monitoring technique described here detects the wear-related data in the measured signal using the WPT and FDR. This is a component-level approach to extracting features from a measured signal, as opposed to an energy-based method, which may fail to extract some of the relevant data or features. Furthermore, such a component-level approach provides specific information on faults in the signal (wear-related faults or sensitive positions as well as the progress of a fault that is related to tool wear).

Using this method, the optimal and second-best bases can be used to identify features throughout the entire range of machining distances, as shown in Fig. 12(a). The optimal and second-best bases could also be used to detect the maximum variations in the measured data as a function of the machining distance.

FDR was used to determine the optimal base for classifying two groups (*i.e.*, machining distances of 0 m and 0.48 m) and the concentration within each group. For the data at a machining distance of 0.08 m, the optimal base point is located near 0 Nm, whereas for a machining distance of 0.48 m, the optimal base point was near -0.04 Nm, and for a machining distance of 0.96 m, the optimal base point was near -0.18 Nm. It follows that the torques selected using the optimal base increased with increasing tool wear.

The green crosses in Fig. 12(a) represent the sensitive points selected using the second-best base (note that because the optimal bases were chosen for machining distances of 0.08 m and 0.48 m, the data at 0.48 m and 0.96 m cannot be better classified than at 0.08 m and 0.48 m). The selected points and ranges represent the variations due to machining distance remarkably well, and hence, they directly reflect the changes in the geometry of the tool.

6.3 Comparison of the component-level method without WPT and the energy method

The component-level method can be executed without WPT. In this

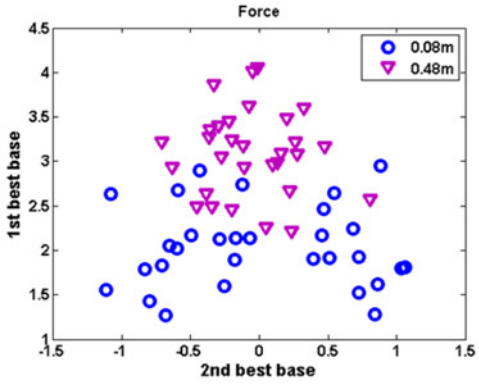

(a) using force data after machining distances of 0.08 m and 0.48 m

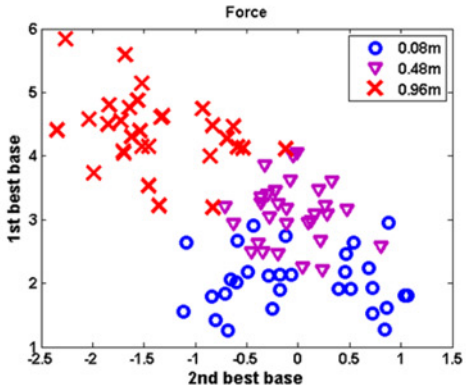

(b) using force data after machining distances of 0.08 m, 0.48 m and 0.96 m

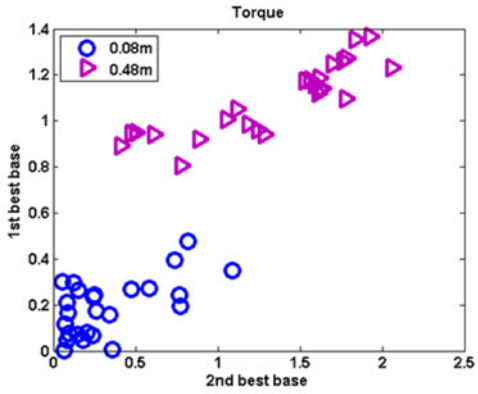

(c) using torque data after machining distances of 0.08 m and 0.48 m

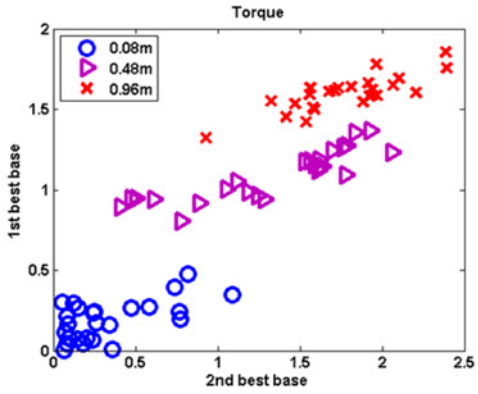

(d) using torque data after machining distances of 0.08 m, 0.48 m and 0.96 m

Fig. 10 Classification results using the proposed condition-monitoring method

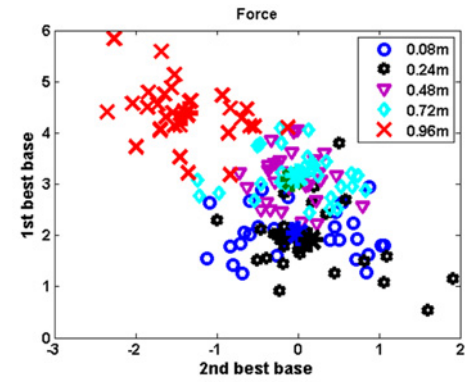

(a)

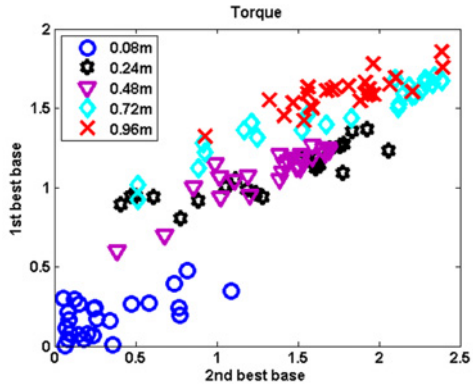

(b)

Fig. 11 Classification results of data at five machining distances: (a) The force signal and (b) the torque signal

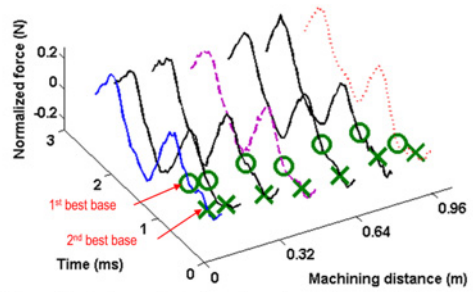

(a) Overall single-period signals and points selected using the optimal (O symbols) and second-best (× symbols) bases using the condition-monitoring method

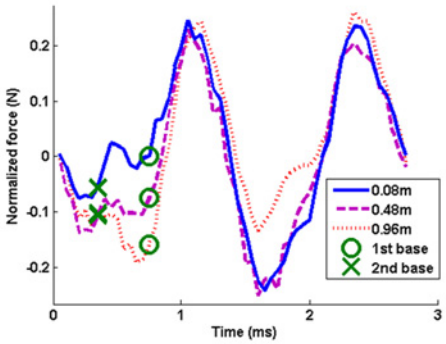

(b) A comparison of the force data at machining distances of 0.08 m, 0.48 m and 0.96 m. The data in the single-period signals selected using the optimal base art marked by green circles

Fig. 12 Component-level analysis

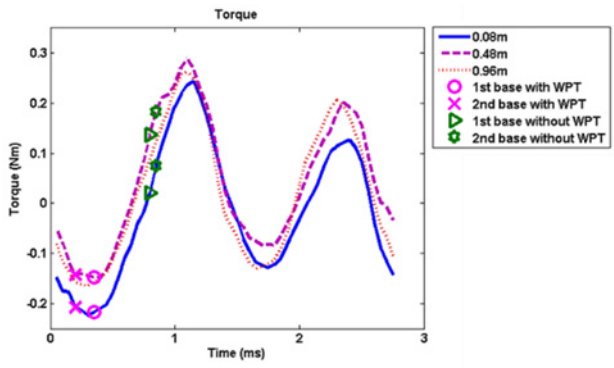

(a)

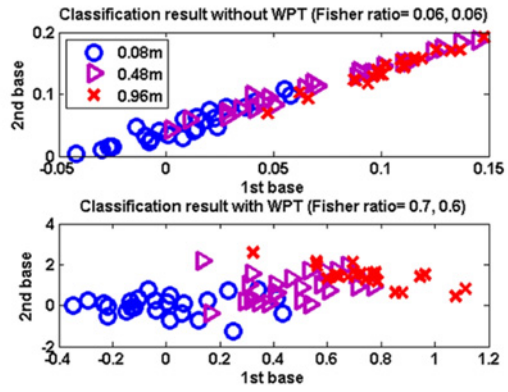

(b)

Fig. 13 Classification results with and without WPT: (a) The sensitive points selected via the component-level method with WPT (pink O and X marks) as well as without WPT (green triangle and star marks), (b) The classification results with and without WPT

case, FDR was applied to each point of the raw signal to determine the sensitive points depending on increased wear or machining distance. Fig. 13(a) shows the sensitive points selected via the component-level method with and without WPT.

With WPT, the peaks were in the sensitive range depending on the machining distance; however, without WPT, points on the inclined side were selected as sensitive points. The classification results are shown in Fig. 13(b). Without WPT, the features at each machining distance overlapped. In particular, with a machining distance of 0.48 m, the data cannot be classified without WPT. However, with WPT, three states were classified that exhibited higher FDRs than the results without WPT.

The energy method with WPT can be used to determine sensitive node energies for tool wear monitoring. The measured signals are classified into low- and high-frequency ranges for WPT, and the wavelet packet energy of each node is calculated as follows:

$$E_j = \frac{1}{T}\sum_{k=1}^{T} d_j^2(k) \tag{15}$$

where T is the length of a node, d_j is the wavelet coefficients of the node, and j is the index of the node in the level. The wavelet packet energies of each node were compared as a function of machining distance and used to select sensitive nodes as features for tool wear monitoring. Because the energy method involves large datasets, the time for the calculation increased compared with the component-level

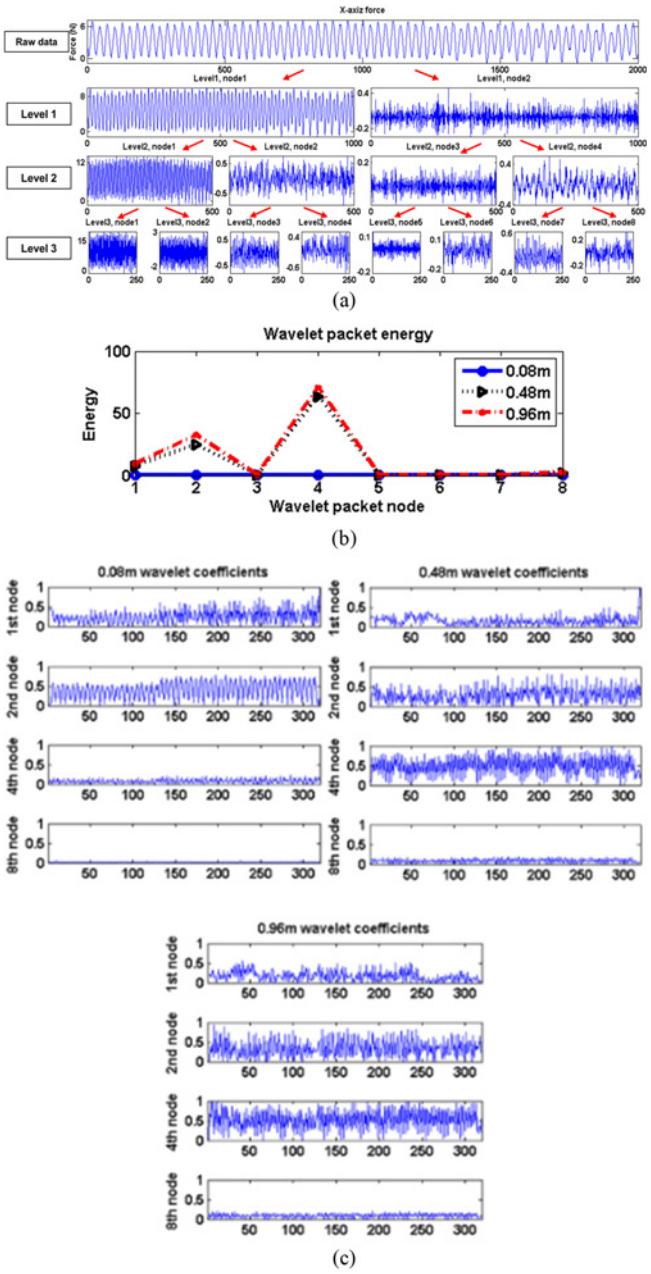

Fig. 14 Condition-monitoring process based on the energy method: (a) Decomposition of the torque data using WPT, (b) comparison of the wavelet packet energies of each node in level 3, and (c) selection of features as a function of the machining distance

model, and sensitive points or features in the raw signal may be lost because of the small SNR.

Fig. 14 shows the monitoring process based on the energy method with WPT. The torque signal was classified according to frequency range using WPT, and the energy of each node in level 3 (the final level) was calculated using Eq. (15). As shown in Fig. 14(b), the 1st, 2nd, 4th, and 8th nodes exhibited prominent variations as a function of the machining distance. Fig. 14(c) shows the coefficients of the sensitive nodes for each machining distance (0.08 m, 0.48 m, and 0.96 m); these features were used for tool state decision making using the energy method.

Table 3 Tool states depending on the tool wear

Tool state	Normal	Medium wear	Excessive wear
Wear	<10 μm	10~20 μm	>20 μm
Image	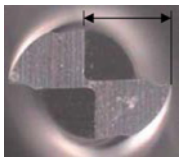	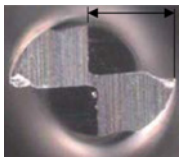	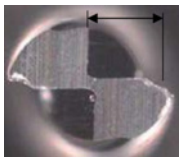

6.4 Predictive results using HMM

Here, we consider three tool states defined by the level of wear: normal (<10 μm of wear), medium (10~20 μm of wear), and excessive (>20 μm of tool wear), as listed in Table 3. The immoderately worn part of the two flutes was measured.

The extracted features were applied to an HMM for state recognition. The recognition performance was determined by the recognition rate, *i.e.*,

$$\textit{Correctly classified states} / (\textit{Misclassified states} + \textit{Correctly classified states}) \times 100 \quad [\%] \tag{16}$$

With the same machining conditions, two sets of machining data are used to train the HMM (*i.e.*, tools 1 and 8, representing normal and early failure modes, respectively). The recognition rates are listed in Table 4. Three monitoring methods were used: component-level analysis without WPT (type I), energy method analysis (type II), and component-level analysis with WPT (type III). The recognition rates are listed in Table 4. With the same machining conditions, tools 2 and 3 exhibited early shank run-out and short tool life, and the recognition rates were lower than those of the normal group for all three methods. The self-recognition rate was also lower for the early failure group than for the normal group. The technique using WPT exhibited higher recognition rates than did the other monitoring methods.

The results obtained with different machining conditions are listed in Table 5. The training data were mild and severe machining conditions, *i.e.*, tools 1 and 7, respectively. Tools 2 and 3 were also in the early failure group under these machining conditions, and the recognition rates were lower than those of the normal group. The results of Table 5 show that the monitoring method with component-level analysis with WPT can predict the wear state of a micro-end mill more effectively than the energy method and component-level method without WPT can.

Component-level analysis with WPT exhibited a higher recognition rate using HMM compared with the energy and component-level methods without WPT. Furthermore, early failure of a micro-end mill (which results primarily from shank run-out) can be predicted more effectively using the component-level analysis with WPT.

7. Conclusions

We have described a tool wear monitoring method for micro-end milling based on single-period signals using WPT and FDR. Shank run-out affects not only the rotational behavior of a micro-end mill but also the tool life and wear imbalance (which induces imbalance torque between the edges of an end mill with two flutes). As a result,

Table 4 The machining conditions (identical conditions)

Tool No.	Cutting speed (m/min)	Feed/tooth (mm)	Run-out (μm)	Lifespan (m)	Note	Recognition rate (%)		
						I	II	III
1	35	0.005	7.9	0.24	Train	82.1	85.3	93.5
2			8.4	0.48	Test	53.3	69.3	78
3			7.4	0.40	Test	59.3	80.5	83.3
4			6.5	0.96	Test	89	79.5	83.3
5			5.6	0.96	Test	68.3	66.7	91.7
6			5.9	0.96	Test	69.7	66.9	89
7			6.6	0.96	Test	72.1	75.3	83.3
8			5.1	0.96	Train	90.2	93.6	100
Total						68.6	73.0	84.8

Table 5 The machining conditions (different machining conditions)

Tool No.	Cutting speed (m/min)	Feed/tooth (mm)	Run-out (μm)	Lifespan (m)	Note	Recognition rate (%)		
						I	II	III
1	35	0.005	6.7	0.74	Train	68.6	73.0	84.8
2	30	0.005	7.2	0.40	Test	67.9	72.6	83
3	30	0.003	8.4	0.56	Test	60	70.6	85.3
4	30	0.003	5.3	0.96	Test	90	70.9	90
5	30	0.001	5.6	0.96	Test	60	73.7	83.7
6	25	0.003	6.4	0.96	Test	61	76.3	91.7
7	25	0.001	6.8	0.96	Train	87.2	95.8	100
Total						67.8	72.8	86.7

excessive shank run-out decreases the tool life and increases tool wear in the initial stages of milling.

A tool wear monitoring method was developed using the WPT and FDR based on single-period signals. A procedure for selecting the optimal base (which includes the daughter wavelet, level, node, and translation) for state classification was described. This method (both with and without WPT) was compared with the energy method in terms of state recognition efficiency with machining conditions and tool life. We find that the proposed tool wear monitoring technique classifies and recognizes the tool state more effectively than the other methods do, including differences in micro-end mill tool lifetimes. Above this diagnosis technique could be applied to the various diameter and tool material, because it use only the vibration sensor and shank displacement data.

ACKNOWLEDGEMENTS

This work was supported by a National Research Foundation (NRF) grant funded by the Ministry of Education, Science, and Technology (No. NRF-2015R1A2A1A13027910), Korea Basic Science Institute (KBSI) Creative Convergence Research Project (CAP-PBF087) funded by the National Research Council of Science and Technology, and the Brain Korea 21 Plus Project in Seoul National University.

REFERENCES

1. Pham, M.-Q., Yoon, H.-S., Khare, V., and Ahn, S.-H., "Evaluation of Ionic Liquids as Lubricants in Micro Milling-Process Capability and Sustainability," Journal of Cleaner Production, Vol. 76, pp. 167-173, 2014.
2. Ritou, M., Garnier, S., Furet, B., and Hascoet, J.-Y., "A New Versatile In-Process Monitoring System for Milling," International Journal of Machine Tools and Manufacture, Vol. 46, No. 15, pp. 2026-2035, 2006.
3. Shao, H., Shi, X., and Li, L., "Power Signal Separation in Milling Process based on Wavelet Transform and Independent Component Analysis," International Journal of Machine Tools and Manufacture, Vol. 51, No. 9, pp. 701-710, 2011.
4. Yoon, H.-S., Lee, J.-Y., Kim, M.-S., and Ahn, S.-H., "Empirical Power-Consumption Model for Material Removal in Three-Axis Milling," Journal of Cleaner Production, Vol. 78, pp. 54-62, 2014.
5. Yoon, H.-S., Kim, E.-S., Kim, M.-S., Lee, J.-Y., Lee, G.-B., and Ahn, S.-H., "Towards Greener Machine Tools-A Review on Energy Saving Strategies and Technologies," Renewable and Sustainable Energy Reviews, Vol. 48, pp. 870-891, 2015.
6. Yoon, H.-S., Wu, R., Lee, T.-M., and Ahn, S.-H., "Geometric Optimization of Micro Drills using Taguchi Methods and Response Surface Methodology," Int. J. Precis. Eng. Manuf., Vol. 12, No. 5, pp. 871-875, 2011.
7. Yoon, H.-S., Lee, J.-Y., Kim, H.-S., Kim, M.-S., Kim, E.-S., et al., "A Comparison of Energy Consumption in Bulk Forming, Subtractive, and Additive Processes: Review and Case Study," Int. J. Precis. Eng. Manfu.-Green Tech., Vol. 1, No. 3, pp. 261-279, 2014.
8. Kim, J.-W., Yoon, H.-S., Lee, H.-S., Lee, K.-E., and Ahn, S.-H., "Defects of Wave Patterns from Tungsten Carbide/Stainless Steel Brazed Micro-End-Milling for Printed Circuit Board Machining,"

Proceedings of the Institution of Mechanical Engineers, Part B: Journal of Engineering Manufacture, Vol. 227, No. 11, pp. 1743-1747, 2013.

9. Yoon, H.-S., Moon, J.-S., Pham, M.-Q., Lee, G.-B., and Ahn, S.-H., "Control of Machining Parameters for Energy and Cost Savings in Micro-Scale Drilling of PCBs," Journal of Cleaner Production, Vol. 54, pp. 41-48, 2013.
10. Kim, J.-W., Yoon, H.-S., and Ahn, S.-H., "Effect of Repeated Insertions into a Mesoscale Pinhole Assembly: Case of Interference Fit," Int. J. Precis. Eng. Manuf., Vol. 14, No. 9, pp. 1651-1654, 2013.
11. Marinescu, I. and Axinte, D. A., "A Critical Analysis of Effectiveness of Acoustic Emission Signals to Detect Tool and Workpiece Malfunctions in Milling Operations," International Journal of Machine Tools and Manufacture, Vol. 48, No. 10, pp. 1148-1160, 2008.
12. Jemielniak, K., Kossakowska, J., and Urbañski, T., "Application of Wavelet Transform of Acoustic Emission and Cutting Force Signals for Tool Condition Monitoring in Rough Turning of Inconel 625," Proceedings of the Institution of Mechanical Engineers, Part B: Journal of Engineering Manufacture, Vol. 225, No. 1, pp. 123-129, 2011.
13. Yun, H. T., Heo, S., Lee, M. K., Min, B.-K., and Lee, S. J., "Ploughing Detection in Micromilling Processes using the Cutting Force Signal," International Journal of Machine Tools and Manufacture, Vol. 51, No. 5, pp. 377-382, 2011.
14. Wang, L., Mehrabi, M. G., and Kannatey-Asibu, E., "Hidden Markov Model-based Tool Wear Monitoring in Turning," Journal of Manufacturing Science and Engineering, Vol. 124, No. 3, pp. 651-658, 2002.
15. Bai, Q. S., Yang, K., Liang, Y. C., Yang, C. L., and Wang, B., "Tool Runout Effects on Wear and Mechanics Behavior in Microend Milling," Journal of Vacuum Science & Technology B, Vol. 27, No. 3, pp. 1566-1572, 2009.
16. Miyaguchi, T., Masuda, M., Takeoka, E., and Iwabe, H., "Effect of Tool Stiffness Upon Tool Wear in High Spindle Speed Milling using Small Ball End Mill," Precision engineering, Vol. 25, No. 2, pp. 145-154, 2001.
17. Stephenson, D. A. and Agapiou, J. S., "Metal Cutting Theory and Practice," CRC Press, pp. 313-330, 2006.
18. Lee, K., Ahn, S. H., Dornfeld, D. A., and Wright, P. K., "The Effect of Run-Out on Design for Manufacturing in Micro-Machining Process," Proc. of the ASME International Mechanical Engineering Congress and Exposition, New York, USA, 2001.
19. Mallat, S. G., "A Wavelet Tour of Signal Processing," Academic Press, pp. 13-15, 1999.
20. Zhu, K., Wong, Y. S., and Hong, G. S., "Wavelet Analysis of Sensor Signals for Tool Condition Monitoring: A Review and Some New Results," International Journal of Machine Tools and Manufacture, Vol. 49, No. 7, pp. 537-553, 2009.
21. Rabiner, L. R. and Juang, B.-H., "An Introduction to Hidden Markov Models," IEEE ASSP Magazine, Vol. 3, No. 1, pp. 4-16, 1986.
22. Zhu, K., San Wong, Y. S., and Hong, G. S., "Multi-Category Micro-Milling Tool Wear Monitoring with Continuous Hidden Markov Models," Mechanical Systems and Signal Processing, Vol. 23, No. 2, pp. 547-560, 2009.
23. Rabiner, L. R., "A Tutorial on Hidden Markov Models and Selected Applications in Speech Recognition," Proceedings of the IEEE, Vol. 77, No. 2, pp. 257-286, 1989.
24. Bicego, M., Pe, E., Tax, D. M. J., and Duin, R. P. W., "Component-based Discriminative Classification for Hidden Markov Models," Pattern Recognition, Vol. 42, No. 11, pp. 2637-2648, 2009.
25. Ertunc, H. M., Loparo, K. A., and Ocak, H., "Tool Wear Condition Monitoring in Drilling Operations using Hidden Markov Models (HMMs)," International Journal of Machine Tools and Manufacture, Vol. 41, No. 9, pp. 1363-1384, 2001.
26. Hong, Y.-S., Ahn, S.-H., Song, C.-K., and Cho, Y.-M., "Component-Level Fault Diagnostics of a Bevel Gear using a Wavelet Packet Transform," Proceedings of the Institution of Mechanical Engineers, Part E: Journal of Process Mechanical Engineering, Vol. 225, No. 1, pp. 1-12, 2011.